Direct Least Squares Estimation of Spatiotemporal Distributions from Dynamic Cardiac SPECT Projections [1]

BW Reutter[†], *Member, IEEE*; GT Gullberg[‡], *Senior Member, IEEE*;
and RH Huesman[†], *Senior Member, IEEE*

[†]Center for Functional Imaging, Lawrence Berkeley National Laboratory
University of California, Berkeley, CA 94720, USA
[‡]Medical Imaging Research Laboratory, Department of Radiology
University of Utah, Salt Lake City, UT 84132, USA

Abstract

Artifacts can result when reconstructing a dynamic image sequence from inconsistent, as well as insufficient and truncated, cone beam SPECT projection data acquired by a slowly rotating gantry. The artifacts can lead to biases in kinetic model parameters estimated from time-activity curves generated by overlaying volumes of interest on the images. However, the biases in time-activity curve estimates and subsequent kinetic parameter estimates can be reduced significantly by first modeling the spatial and temporal distribution of the radiopharmaceutical throughout the projected field of view, and then estimating the time-activity curves directly from the projections. This approach is potentially useful for clinical SPECT studies involving slowly rotating gantries, particularly those using a single-detector system or body contouring orbits with a multi-detector system.

We have implemented computationally efficient methods for fully 4-D direct estimation of spatiotemporal distributions from dynamic cone beam SPECT projection data. Temporal splines were used to model the time-activity curves for the blood pool and tissue volumes in a simulated cardiac data acquisition. Least squares estimates of time-activity curves were obtained quickly and accurately using a workstation. From these curves, kinetic parameters were estimated accurately for noiseless data and with some bias for noisy data.

I. INTRODUCTION

Conventional analysis of dynamically acquired nuclear medicine data involves fitting kinetic models to time-activity curves generated by overlaying volumes of interest on a temporal sequence of reconstructed images. Since dynamic single photon emission computed tomography (SPECT) data acquisition involves gantry motion and the distribution of radiopharmaceutical changes during the acquisition (Figure 1), projections at different angles come from different tracer distributions. Images reconstructed from these inconsistent projections can contain artifacts that lead to biases in the estimated kinetic model parameters. If the data are acquired using cone beam collimators wherein the gantry rotates so that the focal point of the collimators always remains in a plane, additional biases can arise from images reconstructed using insufficient, as well as truncated, projection samples.

To overcome these problems, we and others have been investigating the estimation of time-activity curves and kinetic model parameters directly from dynamic SPECT projection data by modeling the spatial and temporal distribution of the radiopharmaceutical throughout the projected field of view [1]. This approach is potentially useful for clinical studies, particularly in those clinics which have only single-detector systems and thus are not able to perform rapid tomographic acquisitions. Even with a three-detector system, a patient study that utilizes body contouring orbits can take 45–60 sec to obtain one full tomographic acquisition. Thus, the estimation of time-activity curves and kinetic model parameters directly from projection data may also be useful for multi-detector systems acquiring data with a slowly rotating gantry.

Building on research by Carson [2] and by Formiconi [3] into direct time-activity curve estimation for regions of interest, we have used simulated volumetric data to show that unbiased kinetic parameter estimates for one-compartment models can be obtained directly from dynamic SPECT projections, given the blood input function and the proper segmentation of volumes encompassing the projected field of view [4, 5]. We have also applied these methods to a ^{99m}Tc-teboroxime patient study for which the blood input was estimated directly from the projections and the volumes of the left ventricular myocardium, blood pool, liver, and background tissue were determined by automatically segmenting a dynamic image sequence reconstructed from the inconsistent projection data [6].

Here we present a study of the biases that result from modeling various orders of temporal continuity when estimating time-activity curves directly from dynamic cone beam SPECT projection data. Piecewise cubic, quadratic,
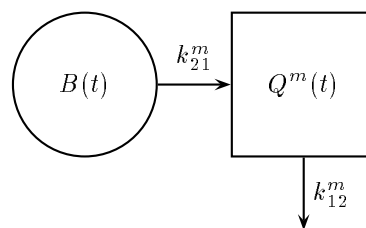

Figure 1: One-compartment kinetic model for ^{99m}Tc-teboroxime in the myocardium. $B(t)$ is the blood input function, $Q^m(t)$ is the tracer in tissue volume m, and k_{21}^m and k_{12}^m are the rate constants for uptake and washout, respectively.

linear, and constant B-splines [7] are used to model the time-activity curves for the blood input, three myocardial volumes of interest, liver, and background tissue in simulated data. Attenuation and geometric point response are modeled, but scatter is not. Segmented volumes encompassing the projected field of view are modeled to contain spatially uniform activity concentrations. Computationally efficient methods are developed which extend Formiconi's least squares algorithm [3] so that fully four-dimensional (4-D) direct spatiotemporal distribution estimation from projections can be performed on a workstation with a modest amount of memory. Using a Monte Carlo simulation, we study also the effects of noisy projections on kinetic parameter estimates for one-compartment models obtained from the spline time-activity curves for the blood input function and the three myocardial volumes of interest.

II. COMPUTATIONALLY EFFICIENT ESTIMATION OF SPATIOTEMPORAL DISTRIBUTIONS DIRECTLY FROM PROJECTIONS

Time varying activity concentrations within volumes of interest encompassing the projected field of view can be modeled by selecting a set of temporal basis functions capable of representing typical time variations and having desired smoothness properties. Similarly, the spatially nonuniform activity concentration within a volume can be modeled by selecting an appropriate set of spatial basis functions defined within the volume. Given a set of temporal basis functions and sets of spatial basis functions for the volumes, coefficients for the resulting spatiotemporal basis functions can be estimated directly from the projections as follows.

The projection of the mth spatial basis function along ray i at angle j is denoted by u_{ij}^m, and the integral of the nth temporal basis function during the time interval associated with angle j of rotation k is denoted by v_{jk}^n. The projection equations can be expressed as

$$p_{ijk} = \sum_{m=1}^{M} \sum_{n=1}^{N} a_{mn} u_{ij}^m v_{jk}^n, \qquad (1)$$

where M is the number of spatial basis functions and N is the number of temporal basis functions. The criterion which is minimized by varying the linear coefficients a_{mn} associated with the time integrals of the projections of the spatiotemporal basis functions is the weighted sum of squares function

$$\chi^2 = \sum_{i=1}^{I} \sum_{j=1}^{J} \sum_{k=1}^{K} \frac{(p_{ijk}^* - p_{ijk})^2}{W_{ijk}}, \qquad (2)$$

where the p_{ijk}^* are the measured projections, the W_{ijk} are weighting factors, I is the number of projection rays per angle, J is the number of angles per rotation, and K is the number of rotations. Typically, the weighting factors are either unity for an unweighted fit or the estimated variances of the projections for a weighted fit.

Equations (1) and (2) can be rewritten in matrix form as

$$\mathbf{p} = \mathbf{Fa}, \qquad (3)$$

$$\chi^2 = (\mathbf{p}^* - \mathbf{Fa})^\text{T} \mathbf{W} (\mathbf{p}^* - \mathbf{Fa}), \qquad (4)$$

respectively, where $\mathbf{p}$ is an IJK element column vector whose $[i + (j-1)I + (k-1)IJ]^\text{th}$ element is p_{ijk}, $\mathbf{F}$ is an $IJK \times MN$ matrix whose $\{[i + (j-1)I + (k-1)IJ], [m + (n-1)M]\}^\text{th}$ element is $u_{ij}^m v_{jk}^n$, $\mathbf{a}$ is an MN element column vector whose $[m+(n-1)M]^\text{th}$ element is a_{mn}, $\mathbf{p}^*$ is an IJK element column vector whose $[i + (j-1)I + (k-1)IJ]^\text{th}$ element is p_{ijk}^*, and $\mathbf{W}$ is an $IJK \times IJK$ diagonal matrix whose $[i + (j-1)I + (k-1)IJ]^\text{th}$ diagonal element is $1/W_{ijk}$. The criterion, χ^2, is minimized by the spatiotemporal basis function coefficients

$$\hat{\mathbf{a}} = (\mathbf{F}^\text{T} \mathbf{W} \mathbf{F})^{-1} \mathbf{F}^\text{T} \mathbf{W} \mathbf{p}^*. \qquad (5)$$

Storing all $IJKMN$ elements of $\mathbf{F}$ and calculating the symmetric matrix $\mathbf{F}^\text{T} \mathbf{W} \mathbf{F}$ using straightforward matrix multiplication is computationally inefficient. For an unweighted least squares reconstruction of the spatiotemporal basis function coefficients $\hat{\mathbf{a}}$ (i.e., for $\mathbf{W}$ an identity matrix), calculating the symmetric matrix $\mathbf{F}^\text{T} \mathbf{F}$ using straightforward matrix multiplication requires $IJKMN(MN + 1)/2$ multiply-and-add operations, given $\mathbf{F}$.

The burden of storing the matrix $\mathbf{F}$ can be reduced significantly by storing instead the spatial basis projection factors u_{ij}^m and the temporal basis integral factors v_{jk}^n and calculating the elements of $\mathbf{F}$ as needed. For $IJM \gg JKN$, this reduces memory usage by a factor of about KN.

For an unweighted least squares reconstruction of the spatiotemporal basis function coefficients $\hat{\mathbf{a}}$ (i.e., for $\mathbf{W}$ an identity matrix), the symmetric $MN \times MN$ matrix $\mathbf{F}^\text{T} \mathbf{F}$ can be calculated more efficiently as follows. Denoting the $\{[m + (n-1)M], [m' + (n'-1)M]\}^\text{th}$ element of $\mathbf{F}^\text{T} \mathbf{F}$ by $\phi^{mnm'n'}$, one has

$$\phi^{mnm'n'} = \sum_{i=1}^{I} \sum_{j=1}^{J} \sum_{k=1}^{K} u_{ij}^m v_{jk}^n u_{ij}^{m'} v_{jk}^{n'}. \qquad (6)$$

Rearranging the summations yields

$$\phi^{mnm'n'} = \sum_{j=1}^{J} \left[\sum_{i=1}^{I} u_{ij}^m u_{ij}^{m'} \right] \left[\sum_{k=1}^{K} v_{jk}^n v_{jk}^{n'} \right] = \sum_{j=1}^{J} \mu_j^{mm'} \nu_j^{nn'}, \qquad (7)$$

where $\mu_j^{mm'}$ and $\nu_j^{nn'}$ denote the inner products $\sum_{i=1}^{I} u_{ij}^m u_{ij}^{m'}$ and $\sum_{k=1}^{K} v_{jk}^n v_{jk}^{n'}$, respectively.

The number of $\mu_j^{mm'}$ factors is $JM(M + 1)/2$, the number of $\nu_j^{nn'}$ factors is $JN(N + 1)/2$, and the number of $\phi^{mnm'n'}$ factors is $MN(MN + 1)/2$. It takes I multiply-and-add operations to calculate each $\mu_j^{mm'}$ factor and K multiply-and-add operations to calculate each $\nu_j^{nn'}$ factor. Given the $\mu_j^{mm'}$ and $\nu_j^{nn'}$ factors, it takes J multiply-and-adds to calculate each
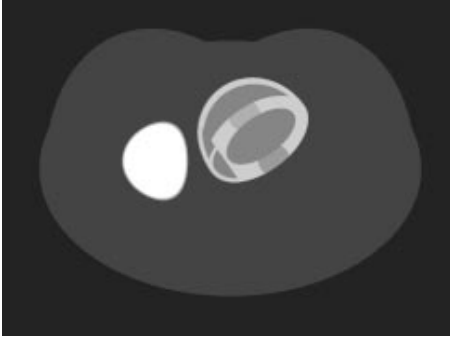
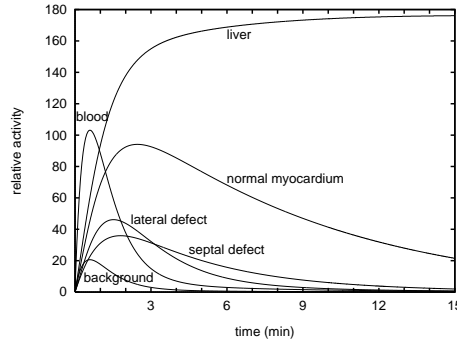Figure 2: Transverse cross section through MCAT emission phantom.

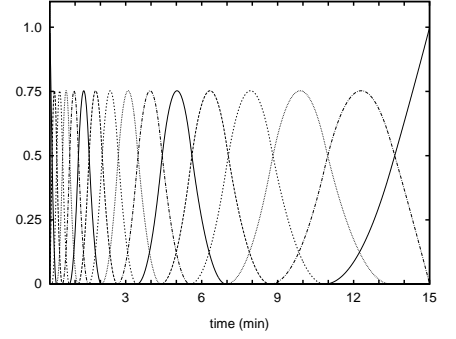Figure 3: Simulated time-activity curves for volumes in Figure 2.

Figure 4: Example of quadratic B-spline temporal basis functions.

of the $\phi^{mnm'n'}$ factors. Thus, the $\phi^{mnm'n'}$ can be calculated using just $J[IM(M+1) + KN(N+1) + MN(MN+1)]/2$ multiply-and-adds. For $I \gg N^2$ and $K < M^2$, this reduces the number of operations by a factor of about KN^2.

Having addressed the major issues of storing $\mathbf{F}$ and calculating $\mathbf{F}^T\mathbf{F}$, the next computational hurdle is calculating $\mathbf{F}^T\mathbf{p}^*$. This can be done in $(I+1)JKMN$ multiply-and-add operations, given the u_{ij}^m and v_{jk}^n factors. The system of equations $\mathbf{F}^T\mathbf{F}\hat{\mathbf{a}} = \mathbf{F}^T\mathbf{p}^*$ can then be solved efficiently for the spatiotemporal basis function coefficients $\hat{\mathbf{a}}$ using the Cholesky decomposition of $\mathbf{F}^T\mathbf{F}$.

III. COMPUTER SIMULATIONS

The Mathematical Cardiac Torso (MCAT) phantom [8], developed by the University of North Carolina Medical Imaging Research Laboratory, was used in a simulation to evaluate the ability to estimate spatiotemporal distributions directly from dynamic cone beam SPECT projections using unweighted least squares. Kinetic parameters for one-compartment models (Figure 1) were estimated from the resulting spatiotemporal distributions, as well. The MCAT emission phantom (Figure 2) contained three myocardial volumes of interest (normal myocardium, septal defect, and lateral defect), blood pool, liver, and background tissue. The myocardial defects were defined as the intersection of 3 cm diameter spheres with the septal and lateral walls of the left ventricle. Projections were attenuated using the corresponding MCAT attenuation phantom. The simulated time-activity curves for the six emission volumes are shown in Figure 3. The time-activity curves for the three myocardial volumes of interest and the liver were generated by using the blood pool curve as the input to one-compartment models having kinetics corresponding to those of teboroxime [9]. The background tissue activity was proportional to the blood pool activity.

The simulated 15 minute SPECT data acquisition consisted of 64 transverse × 32 axial rays per angle ($I = 2048$), $J = 120$ angles per rotation, and one rotation per minute ($K = 15$) of a single-detector system. The projection bins were 7 mm × 7 mm at the detector, and the detector was 30 cm from the center of the field of view. The cone beam collimators had a focal length of 70 cm, a hole diameter of 2 mm, a length of 4 cm, and were offset 1 cm from the detector. Attenuation and geometric point

response were modeled using a ray-driven projector with line length weighting [10]. Scatter was not modeled.

A. Spatiotemporal Distribution Estimates

The spatial basis functions were defined using the known segmentation of the six emission volumes composing the MCAT phantom (Figure 2). Each emission volume was modeled to contain spatially uniform activity, which yielded $M = 6$ spatial basis functions. The temporal basis functions consisted of $N = 16$ splines spanning 15 time segments having geometrically increasing length (Figure 4). Piecewise cubic, quadratic, linear, and constant B-splines were used with initial time segment lengths ranging between 2.5–60 sec.

The computational benefits of factoring the matrix $\mathbf{F}$ into the spatial basis projection factors u_{ij}^m and the temporal basis integral factors v_{jk}^n were evident in the simulation. Rather than storing its more than 350 million elements, about 1.5 million u_{ij}^m and v_{jk}^n factors were stored instead. The number of multiply-and-adds used to calculate $\mathbf{F}^T\mathbf{F}$ was reduced from over 17 billion to less than 6 million. A set of time-activity curves was estimated directly from the 3.7 million simulated projection samples in about 2.3 min on a 194 MHz MIPS R10000-based Silicon Graphics workstation. The calculations of $\mathbf{F}^T\mathbf{F}$ and $\mathbf{F}^T\mathbf{p}^*$ took about 2.2 sec and 2.2 min, respectively.

Table 1 lists the root mean square (RMS) differences between the simulated time-activity curves and the spline curves estimated directly from noiseless projections, normalized by the RMS values of the simulated curves and expressed as percentages. The temporal spline modeling errors were largest for the septal and lateral defects, which had relatively small spatial supports (Figure 2) and low activity concentrations (Figure 3). Intermediate errors resulted for the blood pool and background, which had larger spatial supports but quickly decaying activity concentrations. The errors were smallest for the normal myocardium and liver, which had larger spatial supports and high activity concentrations throughout the simulated data acquisition. The errors tended to increase as the length of the initial time segment for the splines increased.

For the relatively rapid initial sampling provided by using initial time segment lengths of 2.5, 5, or 10 sec, the errors for all six volumes ranged between 0.02–3.8%, 0.02–1.7%, 0.09–6.2%, and 1.6–64% for the cubic, quadratic, linear, and

	cubic B-spline temporal basis initial time segment length (sec)						quadratic B-spline temporal basis initial time segment length (sec)					
	2.5	5	10	20	40	60	2.5	5	10	20	40	60
blood pool	0.08	0.2	0.6	2.6	9.2	18	0.2	0.2	0.5	2.2	9.4	18
normal myocardium	0.2	0.1	0.1	0.8	1.4	4.1	0.2	0.1	0.09	0.4	1.0	4.2
septal defect	0.4	0.6	0.9	5.3	38	40	0.8	0.5	0.9	5.1	39	42
lateral defect	0.3	0.7	3.8	14	57	50	0.7	0.6	1.7	11	60	53
liver	0.02	0.02	0.04	0.1	0.3	0.4	0.03	0.02	0.03	0.09	0.3	0.5
background	0.08	0.2	0.6	2.3	8.5	16	0.2	0.2	0.5	2.1	8.7	17
	linear B-spline temporal basis initial time segment length (sec)						constant B-spline temporal basis initial time segment length (sec)					
	2.5	5	10	20	40	60	2.5	5	10	20	40	60
blood pool	1.0	0.9	1.1	3.0	11	20	10	9.5	11	13	19	26
normal myocardium	0.5	0.4	0.4	0.5	2.0	5.0	7.5	6.4	6.4	6.2	7.5	8.5
septal defect	3.1	2.7	3.2	11	53	34	64	64	51	56	59	110
lateral defect	6.2	5.7	4.4	6.8	51	60	40	49	39	73	65	110
liver	0.1	0.09	0.09	0.1	0.4	0.6	1.6	1.6	1.6	2.0	3.2	4.0
background	0.9	0.8	1.0	2.8	10	18	9.5	9.0	9.6	12	17	24

Table 1
Percent RMS differences between simulated time-activity curves and time-activity curves estimated directly from noiseless projections.

constant B-splines, respectively. For the uniform time sampling provided by using an initial time segment length of 60 sec, the corresponding errors ranged between 0.4–50%, 0.5–53%, 0.6–60%, and 4.0–110%.

B. Kinetic Parameter Estimates

Of interest is how the temporal spline modeling errors bias the estimates of kinetic parameters obtained from the directly estimated time-activity curves. To study this we used the program RFIT [11, 12, 13] to fit one-compartment kinetic models (Figure 1) to the directly estimated time-activity curves for the three myocardial volumes of interest, using the directly estimated blood pool curve as the input function.

Table 2 lists the kinetic parameter estimates obtained from the spline models for time-activity curves estimated directly from noiseless projections. The biases in the uptake parameters k_{21}^m and the washout parameters k_{12}^m were particularly small when using quadratic B-splines and initial time segment lengths of 2.5, 5, or 10 sec. For these three sets of basis functions, the biases ranged between 0.0–1.0%.

To study the effects of noisy projections on kinetic parameter estimates obtained from spline time-activity curves, 100 realizations of projections having Poisson noise were generated. The simulated blood input function amplitude was adjusted so that about 10 million events were detected using the cone beam collimators. Quadratic B-splines and an initial time segment length of 10 sec (Figure 4) were used to model the time-activity curves. A two-tailed t test was used to assess the biases in the sample means of the kinetic parameter estimates.

Results of the 100 noisy realizations are presented in Table 3. The sample means of the uptake parameter k_{21}^1 and the washout parameter k_{12}^1 for the normal myocardium did not differ significantly from the simulated values ($P > 0.4$). The sample standard deviations were about 1%. The sample means of the uptake and washout parameters for the septal and lateral defects were significantly different from the simulated values ($P < 0.05$). The differences between the sample means and the simulated values ranged between 5–16%. The sample standard deviations ranged between 22–42%.

IV. DISCUSSION

Computational issues associated with fully 4-D direct estimation of spatiotemporal distributions from dynamic cone beam SPECT projection data have been addressed, so that least squares estimates of time-activity curves can be obtained quickly and accurately using a workstation with a modest amount of memory. Temporal B-splines were used to model the time-activity curves for the blood pool and tissue volumes in a simulated cardiac data acquisition. From these curves, kinetic parameters for compartmental models were estimated accurately for noiseless data and with some bias for noisy data.

The methodology presented here facilitates future research into the joint estimation of the blood input function and kinetic parameters for compartmental models directly from projection data, as well as the parameterization of spatially nonuniform activity concentrations within segmented volumes encompassing the projected field of view.

V. ACKNOWLEDGMENTS

		simulated	cubic B-spline temporal basis initial time segment length (sec)						quadratic B-spline temporal basis initial time segment length (sec)					
			2.5	5	10	20	40	60	2.5	5	10	20	40	60
normal	k_{21}^1	0.700	0.700	0.700	0.701	0.700	0.683	0.709	0.701	0.701	0.700	0.700	0.684	0.708
myocardium	k_{12}^1	0.150	0.150	0.150	0.150	0.150	0.149	0.155	0.150	0.150	0.150	0.150	0.149	0.155
septal	k_{21}^2	0.300	0.301	0.301	0.300	0.286	0.181	0.358	0.303	0.302	0.300	0.297	0.183	0.350
defect	k_{12}^2	0.300	0.301	0.301	0.300	0.288	0.207	0.334	0.302	0.301	0.300	0.296	0.211	0.326
lateral	k_{21}^3	0.500	0.498	0.496	0.522	0.441	1.17	2.54	0.502	0.499	0.502	0.444	1.19	2.89
defect	k_{12}^3	0.600	0.599	0.598	0.616	0.565	0.942	1.75	0.602	0.598	0.603	0.561	0.957	1.87

		simulated	linear B-spline temporal basis initial time segment length (sec)						constant B-spline temporal basis initial time segment length (sec)					
			2.5	5	10	20	40	60	2.5	5	10	20	40	60
normal	k_{21}^1	0.700	0.703	0.700	0.702	0.698	0.687	0.708	0.688	0.685	0.681	0.682	0.717	0.641
myocardium	k_{12}^1	0.150	0.150	0.150	0.150	0.150	0.149	0.155	0.146	0.147	0.147	0.148	0.154	0.149
septal	k_{21}^2	0.300	0.295	0.292	0.308	0.301	0.170	0.335	0.317	0.275	0.265	0.379	0.252	0.082
defect	k_{12}^2	0.300	0.297	0.296	0.305	0.302	0.204	0.315	0.341	0.299	0.294	0.322	0.254	0.125
lateral	k_{21}^3	0.500	0.533	0.498	0.491	0.533	1.22	1.90	0.533	0.734	0.665	0.331	1.98	4.23
defect	k_{12}^3	0.600	0.602	0.578	0.585	0.626	0.990	1.32	0.635	0.833	0.660	0.553	1.36	2.09

Table 2

Kinetic parameters obtained from time-activity curves estimated directly from noiseless projections. Units for k_{21}^m and k_{12}^m are min^{-1}.

		simulated	noisy ($n = 100$) sample mean	noisy ($n = 100$) sample std dev
normal	k_{21}^1	0.700	0.700	0.0064
myocardium	k_{12}^1	0.150	0.150	0.0016
septal	k_{21}^2	0.300	0.314*	0.072
defect	k_{12}^2	0.300	0.317*	0.066
lateral	k_{21}^3	0.500	0.578*	0.21
defect	k_{12}^3	0.600	0.653*	0.16

Table 3

Kinetic parameters obtained from time-activity curves estimated directly from 100 realizations of noisy projections (10 million detected events) using quadratic B-spline temporal basis functions and an initial time segment length of 10 sec. Sample means significantly different from the simulated values (i.e., $P < 0.05$ for a two-tailed t test) are labeled with asterisks. Units for k_{21}^m and k_{12}^m are min^{-1}.

VI. REFERENCES

[1] G T Gullberg, R H Huesman, S G Ross, E V R Di Bella, G L Zeng, B W Reutter, P E Christian, and S A Foresti. Dynamic cardiac single-photon emission computed tomography. In B L Zaret and G A Beller, editors, *Nuclear Cardiology: State of the Art and Future Directions*, chapter 11, pages 137–187. Mosby Inc, St Louis, 1999.

[2] R E Carson. A maximum likelihood method for region-of-interest evaluation in emission tomography. *J Comput Assist Tomogr*, 10(4):654–663, 1986.

[3] A R Formiconi. Least squares algorithm for region-of-interest evaluation in emission tomography. *IEEE Trans Med Imag*, 12(1):90–100, 1993.

[4] R H Huesman, B W Reutter, G L Zeng, and G T Gullberg. Kinetic parameter estimation from SPECT cone-beam projection measurements. *Phys Med Biol*, 43(4):973–982, 1998.

[5] B W Reutter, G T Gullberg, and R H Huesman. Kinetic parameter estimation from attenuated SPECT projection measurements. *IEEE Trans Nucl Sci*, 45(6):3007–3013, 1998.

[6] B W Reutter, G T Gullberg, and R H Huesman. Kinetic parameter estimation from dynamic cardiac patient SPECT projection measurements. In R Sudharsanan, editor, *1998 IEEE Nuclear Science Symposium and Medical Imaging Conference Record*, pages 1953–1958, 1999.

[7] R H Bartels, J C Beatty, and B A Barsky. *An Introduction to Splines for Use in Computer Graphics and Geometric Modeling*. M Kaufmann Publishers, Los Altos, California, 1987.

[8] B M W Tsui, J A Terry, and G T Gullberg. Evaluation of cardiac cone-beam single photon emission computed tomography using observer performance experiments and receiver operating characteristic analysis. *Invest Radiol*, 28(12):1101–12, 1993.

[9] R K Narra, T Feld, and A D Nunn. Absorbed radiation dose to humans from technetium-99m-teboroxime. *J Nucl Med*, 33(1):88–93, 1992.

[10] G L Zeng, G T Gullberg, B M W Tsui, and J A Terry. Three-dimensional iterative reconstruction algorithms with attenuation and geometric point response correction. *IEEE Trans Nucl Sci*, 38(2):693–702, 1991.

[11] B M Mazoyer, R H Huesman, T F Budinger, and B L Knittel. Dynamic PET data analysis. *J Comput Assist Tomogr*, 10(4):645–653, 1986.

[12] P G Coxson, E M Salmeron, R H Huesman, and B M Mazoyer. Simulation of compartmental models for kinetic data from a positron emission tomograph. *Comput Methods Programs Biomed*, 37(3):205–214, 1992.

[13] R H Huesman, B L Knittel, B M Mazoyer, P G Coxson, E M Salmeron, G J Klein, B W Reutter, and T F Budinger. Notes on RFIT: A program for fitting compartmental models to region-of-interest dynamic emission tomographic data. Report LBL-37621, Lawrence Berkeley Laboratory, 1993.